JOURNAL OF EXPERIMENTAL AND THEORETICAL PHYSICS, 2024, VOL. 165, No. 1, pp. 18–24

ATOMS, MOLECULES, OPTICS

INTENSE HIGH HARMONIC GENERATION IN FULLERENE MOLECULE C_{180}

© 2024 H. K. Avetissian[a], A. G. Ghazaryan[a]*, H. H. Matevosyan[b], G. F. Mkrtchian[a]

[a]*Centre of Strong Fields Physics at Physics Research Institute, Yerevan State University, Yerevan 0025, Armenia*

[b]*Institute of Radiophysics and Electronics NAS RA, Ashtarak 0203, Armenia*

**e-mail: amarkos@ysu.am*

Received 20.08.2023
Revised 24.09.2023
Accepted 25.09.2023

Abstract. Investigation of high-order harmonic generation (HHG) in the large fullerene C_{180} molecule under intense laser field is presented. To model the C_{180} molecule and its interaction with the laser field, we employ the tight-binding mean-field approach. Our detailed analysis of the HHG power spectrum reveals the multiphoton resonant nature of harmonic generation, shedding light on the underlying quantum processes involved. We examine the dependence of cutoff harmonics on both laser intensity and frequency, providing valuable insights into the optimal conditions for enhancing HHG in C_{180}. We demonstrate that the C_{180} molecule exhibits a significantly stronger high harmonic intensity compared to the more widely studied C_{60} fullerene.

Keywords: graphene quantum dot, intense wave, many particle column interactions, fullerene

DOI: 10.31857/S00444510240101e3

1. INTRODUCTION

One of the fundamental processes in intense lasermatter interaction is high harmonic generation [1,2], which allows for the production of coherent ultraviolet and x-ray radiation in atomic systems. HHG involves highly multiphoton processes [3], offering access to extreme time resolution and enabling attosecond physics [4, 5]. Among nanostructured materials with potential for nonlinear extreme optical applications, carbon allotropes [6,7], such as fullerenes [8], are of particular interest. Fullerenes are large molecules formed by closing a graphite sheet, and their stable closed topological structure makes them intriguing for study. The discovery of fullerene C_{6o} [9] stimulated research into many other fullerene molecules with different symmetries [10–15]. Large fullerenes have since been the subject of active investigation [16–19].

In the field of HHG, enhancing conversion efficiency is crucial, and it strongly depends on the density of emitters and possible excitation channels. Atomic clusters have shown promise in significantly increasing harmonic intensity compared to atomic systems [20–22], leading to a growing interest in extending HHG to graphene quantum dots [23–26], and fullerenes [27,28].

Theoretical studies have predicted strong HHG from both C_{60} and C_{70} molecules [29–33], as well as solid C_{60} [31]. Notably, increasing the number of atoms in fullerene molecules results in more excitation channels that can amplify the HHG signal. Therefore, exploring the HHG process in large fullerenes holds great significance.

In this letter, we present a microscopic theory that investigates the extreme nonlinear interaction of large fullerene C_{180} with strong electromagnetic radiation of linear polarization. We uncover the general structure of the HHG spectrum, including its cutoff dependence on laser intensity/frequency and its relation to molecular excitations. Our findings shed light on the potential of large fullerenes in HHG and open new avenues for further research in this field.

The paper is organized in such a way. In Sec. II presents the basic model of multiphoton excitation and HHG in fullerene Ciso- In Sec. III and IV present the results of the numerical study and conclusions, respectively.

2. THE MODEL

We start by describing the model and theoretical approach. Fullerene C_{180} is assumed to interact with a mid-infrared or visible light laser pulse that excites electron coherent

dynamics. The schematic structure of C_{180} is deployed in Fig. 1. The C_{180} molecule is invariant under the inversion with respect to the center of mass and has icosahedral point group (I_h) symmetry. We assume a neutral C_{180}, which will be described in the scope of the tight-binding (TB) theory. The electron-electron interaction (EEI) is described in the extended Hubbard approximation [32,34,35]. Hence, the total Hamiltonian reads:

$$\widehat{H} = \widehat{H}_0 + \widehat{H}_{\text{int}}, \tag{1}$$

where

$$\widehat{H}_0 = -\sum_{\langle i,j\rangle\sigma} t_{ij} c^{\dagger}_{i\sigma} c_{j\sigma} + \\ + \frac{U}{2}\sum_{i\sigma} n_{i\sigma} n_{i\bar{\sigma}} + \frac{1}{2}\sum_{\langle i,j\rangle} V_{ij} n_i n_j \tag{2}$$

— is the free fullerene Hamiltonian. Here $c^{\dagger}_{i\sigma}$ creates an electron with spin polarization $\sigma = \{\uparrow,\downarrow\}$ at site i ($\bar{\sigma}$ is the opposite to σ spin polarization) and $\langle i,j\rangle$ runs over all the first nearest-neighbor hopping sites with the hopping integral between the nearest-neighbor atoms at positions $\mathbf{r}_i$ and $\mathbf{r}_j$. The hopping integral approximated by

$$t_{ij} = t_0 + \alpha\left(d_0 - \left|\mathbf{r}_i - \mathbf{r}_j\right|\right), \qquad \text{[29, 32]:}$$

where $d_0 = 1.54$ Å, $t_0 = 2.17$ eV, and the electron-lattice coupling constant $\alpha = 3.5$ eV / Å. Input coordinates for the C_{180} are generated with the program Fullerene via a face-spiral algorithm [36]. The initial structure is further optimized by a force Held specifically designed for fullerenes [37]. The second and third terms in (2) describe the EEI Hamiltonian with on-site U and intersite $V_{ij} = 0.5Ud_{min} / d_{ij}$ Coulomb repulsion energies, where d_{min} is the minimal nearest-neighbor distance. The light-matter interaction is described in the lengthgauge

$$\widehat{H}_{\text{int}} = e\sum_{i\sigma} \mathbf{r}_i \cdot \mathbf{E}(t) c^{\dagger}_{i\sigma} c_{i\sigma}, \tag{3}$$

where $\mathbf{E}(t) = f(t)E_0\hat{\mathbf{e}}\cos\omega t$ is the electric field strength, with the amplitude E_0, frequency ω, polarization $\hat{\mathbf{e}}$ unit vector, and pulse envelope $f(t) = \sin^2(\pi t / \mathcal{T})$. The pulse duration $\mathcal{T}$ is taken to be 10 wave cycles: $\mathcal{T} = 20\pi / \omega$. From the Heisenberg equation under the Hartree-Fock approximation one can obtain evolutionary equations for the single-particle density matrix

$$\rho^{(\sigma)}_{ij} = \left\langle c^{\dagger}_{j\sigma} c_{i\sigma} \right\rangle \qquad \text{[32]:}$$

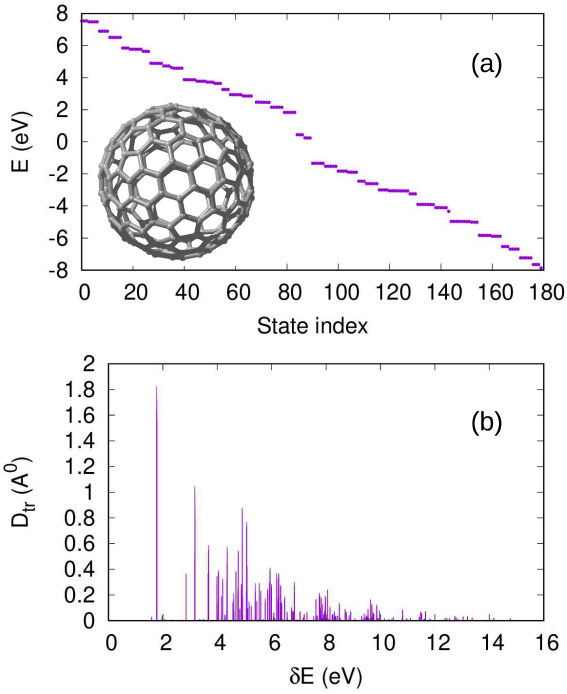

Fig. 1. Eigenenergies of fullerene molecule C_{180} (a) and the absolute value of transition dipole moment matrix elements at interband transitions (b). The inset in (a) is the schematic structure of C_{180}.

$$i\hbar\frac{\partial\rho^{(\sigma)}_{ij}}{\partial t} = \sum_k\left(\tau_{kj\sigma}\rho^{(\sigma)}_{ik} - \tau_{ik\sigma}\rho^{(\sigma)}_{kj}\right) + \\ + \left(V_{i\sigma} - V_{j\sigma}\right)\rho^{(\sigma)}_{ij} + \\ + e\mathbf{E}(t)\left(\mathbf{r}_i - \mathbf{r}_j\right)\rho^{(\sigma)}_{ij} - i\hbar\gamma\left(\rho^{(\sigma)}_{ij} - \rho^{(\sigma)}_{0ij}\right), \tag{4}$$

where $V_{i\sigma}$ and $\tau_{ij\sigma}$ are defined via density matrix $\rho^{(\sigma)}_{ij}$ and its initial value:

$$V_{i\sigma} = \sum_{j\alpha} V_{ij}\left(\rho^{(\alpha)}_{jj} - \rho^{(\alpha)}_{0jj}\right) + U\left(\rho^{(\bar{\sigma})}_{ii} - \rho^{(\bar{\sigma})}_{0ii}\right),$$

$$\tau_{ij\sigma} = t_{ij} + V_{ij}\left(\rho^{(\sigma)}_{ji} - \rho^{(\sigma)}_{0ji}\right).$$

3. RESULTS

First we consider eigenenergies and possible optical transitions of considered system prior the interaction with the strong laser pulse. These results are obtained by numerical diagonalization of the TB Hamiltonian. With the help of the obtained eigenstates $\psi_\mu(i)$ we also calculate the matrix elements of the transition dipole moment:

$$\mathbf{d}_{\mu'\mu} = e\sum_i \psi^*_{\mu'}(i)\mathbf{r}_i\psi_\mu(i).$$

The results for eigenenergies and the absolute value of transition dipole moment matrix elements at interband transitions are shown in Fig. 1. In Fig. 1, we observe that the icosahedral symmetry of C_{180} leads to highly degenerate states with numerous dipole-allowed excitation channels. The optical gap in C_{180} is approximately 1.8 eV, which is narrower than that in C_{60} (2.74 eV). Notably, the transition dipole moment exhibits peaks within the range of 1.8–15 eV, suggesting the presence of efficient multiphoton excitation and subsequent high-energy singlephoton transitions. These factors play a significant role in shaping the high harmonic generation (HHG) spectrum, as we will explore in the following.

To study the HHG process in C_{180} fullerene molecule we evaluate the high-harmonic spectrum by Fourier Transformation of the dipole acceleration,

$$\mathbf{a}(t) = d^2\mathbf{d}(t) / dt^2, \tag{5}$$

where the dipole momentum is defined as

$$\mathbf{d}(t) = e\sum_{i\sigma}\mathbf{r}_t\rho_{ii}^{(\sigma)}(t). \tag{6}$$

Then

$$\mathbf{a}(\Omega) = \int_{-\infty}^{\infty}\mathbf{a}(t)e^{i\Omega t}W(t)dt,$$

and $W(t)$ is the window function to suppress small fluctuations [38] and to decrease the overall background (noise level) of the harmonic signal. As a window function we take the pulse envelope $f(t)$. To obtain the mean picture which docs not depend on the orientation of the molecule with respect to laser polarization, we take the wave polarization unity vector as $\hat{\mathbf{e}} = (1/\sqrt{3})\{1,1,1\}$. The spectra are calculated for moderate Coulomb repulsion energy, $U = 2$ eV. The relaxation rate is taken to be $\hbar\gamma = 0.1$ eV. For the convenience, we normalize the dipole acceleration by the factor $a_0 = e\bar{\omega}^{-2}\bar{d}$, where $\bar{\omega} = 1$ eV/$\hbar$ and $\bar{d} = 1$ Å. The power radiated at the given frequency is proportional to $|\mathbf{a}(\Omega)|^2$. The time propagation of Eq. (4) is performed by the 4-order Runge-Kutta algorithm. As an initial density matrix we take a fully occupied valence band and a completely empty conduction band.

Moving forward, we delve into exploring the dependence of high-order harmonic generation (HHG) on the pump wave frequency within a range of $\hbar\omega = 1 - 2$ eV. In Fig. 2, we illustrate the HHG spectra's frequency dependence, revealing that due to inversion symmetry, only odd harmonics arc generated. Notably, in the cutoff region of high harmonics, a distinctive feature emerges, showcasing the gradual decrease

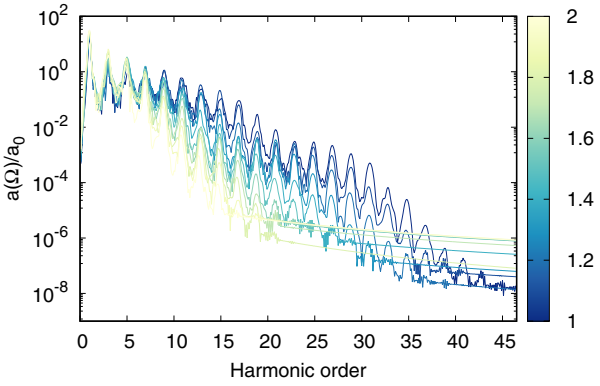

Fig. 2. (Color online) The dependence of the HHG spectra on the wave field frequency is illustrated for C_{180} using the normalized dipole acceleration Fourier transformation, $a(\Omega) / a_0$, plotted on a logarithmic scale. The wave wave intensity is 10 TW/cm^2. The color bar shows the fre-quency of the pump wave in eV/ω

of HHG intensity as the wave field frequency ω increases. It is interesting to observe that the cutoff harmonic position can be approximated by the scaling relation $N_{cut} \propto \omega^{-3/2}$. Comparing this with atomic HHG via the free continuum, where $N_{cut} \propto \omega^{-3}$ [2], we find that for C_{180}, the cutoff harmonic energy ($\hbar\omega N_{cut} \propto \omega^{-1/2}$) decreases at a slower rate as the pump wave photon energy increases.

Conversely, for the low harmonics, we observe an alternating variation with respect to the frequency. This behavior can be attributed to the multiphoton resonant transitions between the valence and conduction bands. This resonant-nature of HHG is further elucidated in Fig. 3, where we depict the dependence of emission strength for the 3rd, 5th, 7th, and 9th harmonics on the pump wave frequency. It is apparent that these harmonics exhibit resonant behavior. Analyzing Fig. 1(b), we observe that the transition dipole moments for interband transitions exhibit peaks around these resonant-frequencies, providing additional support for the multiphoton resonant transitions. For instance, the highest peak for the 3rd harmonic occurs at 1.9 eV, and from Fig. 1(b), we find that the transition dipole moment has a local peak at$3\omega \simeq 5.7$ eV/$\hbar$ with multiple excitation channels. The resonant behavior is further substantiated by the residual population of conduction band energy levels, as depicted in Fig. 4. Here, we plot the population of conduction band energy levels after the interaction, revealing a significant population of levels. This observation further confirms the importance of multiphoton resonant transitions in the HHG process of large fullerene C_{180} under intense near-infrared laser fields.

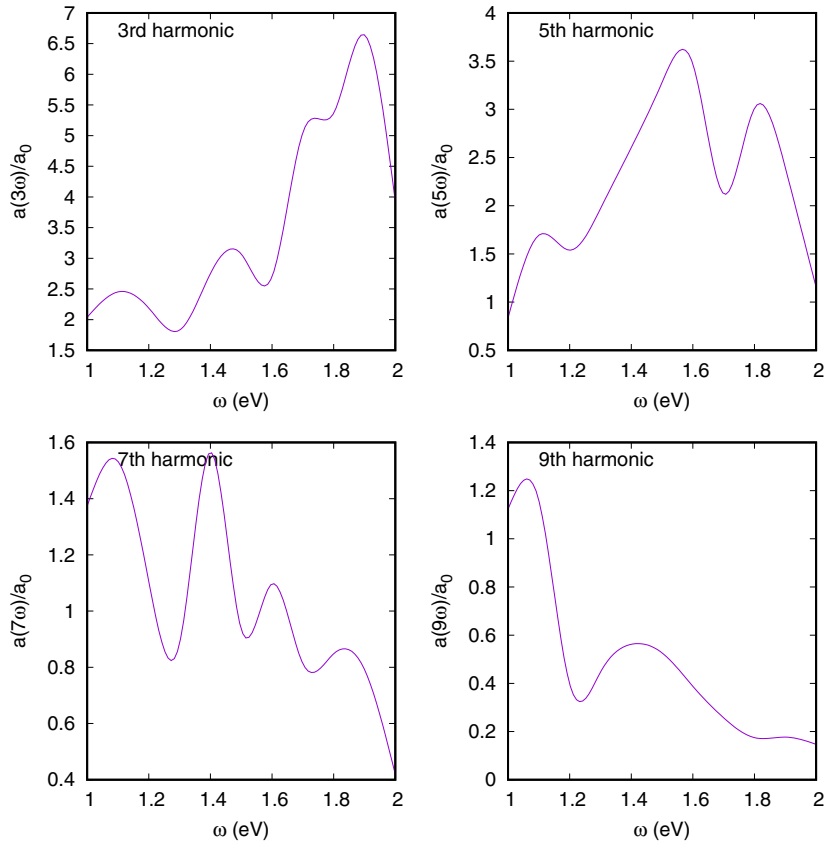

Fig. 3. The dependence of emission strength for the 3rd, 5th, 7th, and 9th harmonics on the pump wave frequency for the setup of Fig. 2.

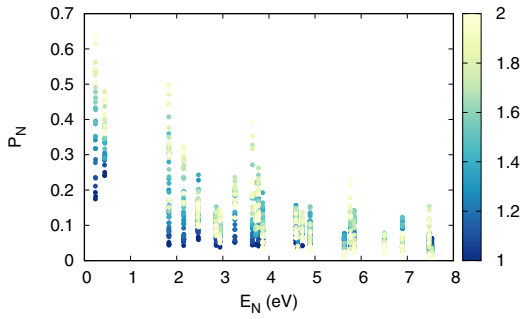

Fig. 4. (Color online) The residual population of conduction band energy levels for the setup of Fig. 2.

Next, we delve into investigating the dependence of the cut-off frequency on the pump wave intensity by analyzing the HHG spectra for different intensities. Fig. 5 presents the HHG spectra's dependence on the wave field amplitude. Unlike HHG in atoms [2], where the cut-off energy is proportional to the wave field intensity, in the case under consideration the cut-off energy tends to saturation for strong laser fields. This trend becomes apparent when looking at the bottom panel of Fig. 5, which shows the relationship between cut-off harmonics and wave intensity (I). The plotted data is accompanied by a fitting function of the form $1^{1/4}$. In the intensity range up to 15 TW/cm^2, there is a good agreement-between the numerical data and the scaling function, which indicates a fairly good approximation. However, it is noteworthy that beyond this intensity, the saturation phenomenon becomes apparent.

Another notable aspect of the HHG signals in fullerene molecules is their dependence on the size of the molecule. To explore this, we compare the HHG signals per particle for C_{180} and C_{60} in Fig. 6. As observed, there is a substantial increase in the HHG signal for C_{180}, a trend also observed for graphene quantum dots in previous studies [23]. This enhancement can be attributed to the density of states, indirectly reflected in Fig. 1 through the transition dipole moments. From Fig. 1, it becomes apparent that C_{180} possesses significantly more transition channels than C_{60}, which contributes to the amplified HHG response. Next, we would like to clarify the procedural aspects of the Fourier transform process. The applied approach includes the numerical solution of equation (1) in which the function $\mathbf{a}(t)$ is discredited

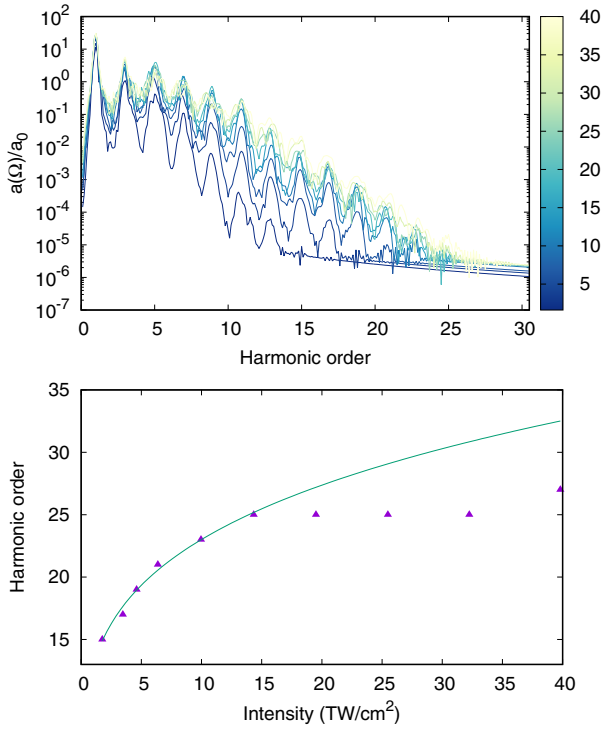

Fig. 5. (Color online) In the top panel the dependencies of the HHG spectra on the wave field amplitude is illustrated for C_{180} using the normalized dipole acceleration Fourier transformation, $a(\Omega) / a_0$ plotted on a logarithmic scale. The pump wave frequency is $\omega = 1.5$ eV/$\hbar$ (wavelength 827 nm). The color bar shows the pump wave intensity in unity TW/cm^2. The lower panel shows the dependence of the cutoff harmonics on the wave intensity together with the approximation function (solid line).

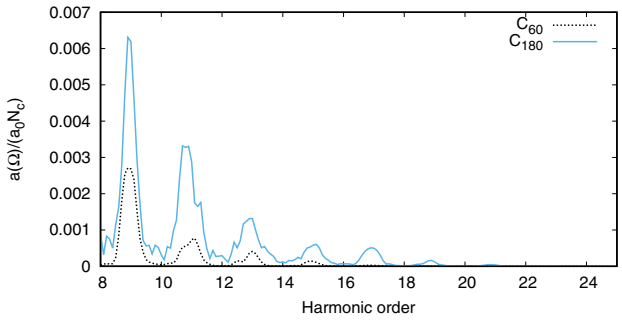

Fig. 6. The comparision of HHG signals per particle for C_{180} and C_{60}. The pump wave frequency is $\omega = 1.5$ eV/$\hbar$ (wavelength 827 nm) and wave intensity is 10 TW/cm^2.

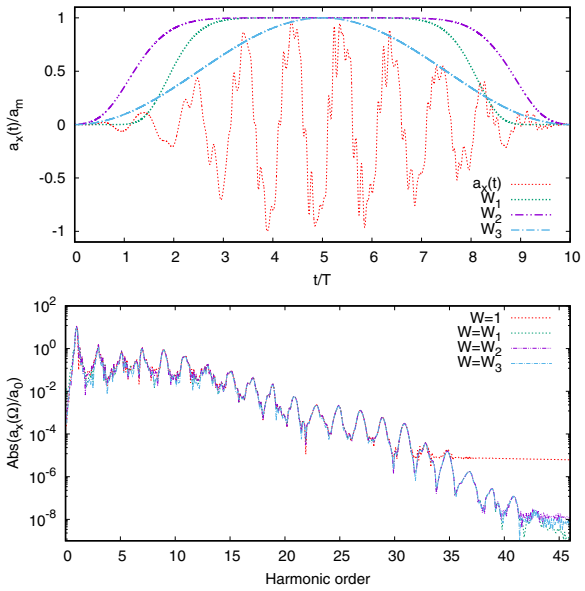

Fig. 7. (Color online) The top panel shows the x-component of the dipole acceleration versus time along with window functions. Wave intensity 10 TW/cm^2, frequency is 1 eV (wavelength 1240 nm). The lower panel shows the SHG spectrum calculated using window functions corresponding to the dipole acceleration in the upper panel.

at regular intervals in the time $[0, \mathcal{T}]$. Before the interaction, $\mathbf{a}(t)$ is zero, and after the interaction, a residual $\mathbf{a}(t)$, resulting from the conserved level populations is negligible. Considering that here the signal takes the form of a continuous function with a limited bandwidth, we resort to an approximation of the continuous Fourier transform by a discrete analog, carried out in the time domain $[0, \mathcal{T}]$, where the field-induced HHG occurs. It is noteworthy that insignificant fluctuations occur at the time boundaries of generation development, which contribute to increased noise within the harmonic signal. This in turn smears harmonic signals towards the end of the spectrum. The most- intense SHG occurs at peak amplitudes of the laser field. This leads to the need to introduce a window function to suppress these minor fluctuations. It was important to clarify that the application of this window function docs not-change the rate of harmonic generation in the remaining part of the spectrum, which is confirmed by our calculations. To illustrate this concept, we have chosen the exponential spectrum from Fig. 2, in particular the one with the highest harmonic cut-off. The X-componcnt of the dipole acceleration $a_x(t)$ is shown in fig. 7. It is scaled around its maximum value and mapped to the appropriate window functions. Wc use three window functions: hypergaussian

$$W_{1,2}(t) = \exp\left\{-\left(\frac{t - \mathcal{T}/2}{\tau_{1,2}}\right)^8\right\}$$

with different parameters $\tau_1 = 13\,fs$, $\tau_2 = 16\,fs$, and the pulse envelope

$$W_3 = \sin^2\left(\frac{t}{\tau_3}\right)$$

with $\tau_3 = 13\,fs$.

Turning to the bottom panel of Fig. 7, we visualize the high harmonic generation spectrum for these window functions by contrasting them with a direct Fourier transform. It is noteworthy that the absence of a window function limits the spectrum of harmonics to the 35th order, which is accompanied by a significant background. However, enabling window functions effectively removes the dominant hum, producing distinct-peaks corresponding to higher harmonics. It can be seen from this illustration that the frequency of the harmonics is practically independent of the features of the window functions. Therefore, any of the mentioned functions can be used in an equivalent way. In the case under study, we chose W_3.

4. CONCLUSION

We have conducted a comprehensive investigation into the extreme nonlinear optical response of large fullerene molecules, with a particular focus on C_{180}, which possesses icosahcdral point group symmetry commonly found in such systems. Our study utilized an accurate quantal calculation of the HHG spectra using a mean-field approach that takes into account manybody Coulomb interaction. By solving the evolutionary equations for the singl-particle density matrix, we revealed resonant effects within the HHG spectra and observed a remarkable enhancement in the HHG yield compared with C_{60}. Unlike atomic HHG, where the cut-off energy is directly proportional to the pump wave intensity, in C_{180}, for mid-infrared or visible light laser pulses, the cut-off energy saturates for high-intensity laser fields, gradually decreasing as a function of the pump wave frequency. This behavior highlights the unique response of large fullerene molecules to intense laser fields, which could open up new possibilities for extreme nonlinear optical applications.

FUNDING

This work was supported by the Science Committee of RA in Frames of Project 24WS-1C004.

REFERENCES

1. P. B. Corkum, Phys. Rev. Lett. 71, 1994 (1993).
2. M. Lewenstein, P. Balcou, M. Y. Ivanov, et al., Phys. Rev. A 49, 2117 (1994).
3. H. K. Avetissian, Relativistic Nonlinear Electrody-namics: The QED Vacuum and Matter in SuperStrong Radiation Fields, 88 (Springer, New York, 2015).
4. P. B. Corkum and F. Krausz, Nature physics 3, 381 (2007).
5. F. Krausz and M. Ivanov, Rev. Mod. Phys. 81, 163 (2009).
6. E. H. Falcao and F. Wudl, Environmental and Clean Technology 82, 524 (2007).
7. S. K. Tiwari, V. Kumar, A. Huczko, et al., Critical Reviews in Solid State and Materials Sciences 41, 257 (2016).
8. R. E. Smalley, Reviews of Modern Physics 69, 723 (1997).
9. H. W. Kroto, J. R. Heath, S. C. O'Brien, et al., Nature 318, 162 (1985).
10. H. Kroto and K. McKay, Nature 331, 328 (1988).
11. D. York, J. P. Lu, and W. Yang, Phys. Rev. B 49, 8526 (1994).
12. G. E. Scuseria, Chem. Phys. Lett. 243, 193 (1995).
13. G. E. Scuseria, Science 271, 942 (1996).
14. S. Itoh, P. Ordejon, D. A. Drabold, and R. M. Martin, Phys. Rev. B 53, 2132 (1996).
15. C. H. Xu and G. E. Scuseria, Chem. Phys. Lett. 262, 219 (1996).
16. P. W. Dunk, N. K. Kaiser, C. L. Hendrickson, et al., Nature Commun. 3, 855 (2012).
17. J. W. Martin, G. J. McIntosh, R. Aru, et al., Carbon 125, 132 (2017).
18. S. Wang, Q. Chang, G. Zhang, et al., Frontiers in Chemistry 8, 607712 (2020).
19. E. Ghavanloo, H. Rai-Tabar, A. Kausar, et al., Physics Reports 996, 1 (2023).
20. T. D. Donnelly, T. Ditmire, K. Neuman, et al., Phys. Rev. Lett. 76, 2472 (1996).
21. C. Vozzi, M. Nisoli, J. Caumes, et al., Appl. Phys. Lett. 86 (2005).
22. O. Smirnova, Y. Mairesse, S. Patchkovski, et al., Nature 460, 972 (2009).
23. B. Avchyan, A. Ghazaryan, K. Sargsyan, and K. V. Sedrakian, JETP 134, 125 (2022).
24. B. R. Avchyan, A. G. Ghazaryan, S. S. Israelyan, and K. V. Sedrakian, J. of Nanophot. 16, 036001 (2022).
25. B. Avchyan, A. Ghazaryan, K. Sargsyan, and K. V. Sedrakian, JETP Letters 116, 428 (2022).
26. S. Gnawali, R. Ghimire, K. R. Maga, et al., Phys. Rev. B 106, 075149 (2022).
27. R. Ganeev, L. E. Bom, J. Abdul-Hadi, et al., Phys. Rev. Lett. 102, 013903 (2009).
28. R. Ganeev, L. E. Bom, M. Wong, et al., Phys. Rev. A 80, 043808 (2009).

29. G. P. Zhang, Phys. Rev. Lett. 95, 047401 (2005).
30. G. P. Zhang and T. F. George, Phys. Rev. A 74, 023811 (2006).
31. G. P. Zhang and Y. H. Bai, Phys. Rev. B 101, 081412(R) (2020).
32. H. K. Avetissian, A. G. Ghazaryan, and G. F. Mkrtchian, Phys. Rev. B 104, 125436 (2021).
33. H. K. Avetissian, S. Sukiasyan, H. H. Matevosyan, and G. F. Mkrtchian, arXiv preprint arXiv:2304.04208 (2023).
34. R. L. Martin and J. P. Ritchie, Phys. Rev. B 48, 4845 (1993).
35. G. Zhang, Phys. Rev. B 56, 9189 (1997).
36. P. W. Fowler and D. E. Manolopoulos, An atlas of fullerenes (Courier Corporation, New York, 2007).
37. P. Schwerdtfeger, L. Wirz, and J. Avery, J. of Com- put. Chem. 34, 1508 (2013).
38. G. P. Zhang, M. S. Si, M. Murakami, et al., Nature Commun. 9, 3031 (2018).